Science of the Total Environment 859 (2023) 160110

Contents lists available at ScienceDirect

Science of the Total Environment

journal homepage: www.elsevier.com/locate/scitotenv

Uncovering a 70-year-old permafrost degradation induced disaster in the Arctic, the 1952 Niiortuut landslide-tsunami in central West Greenland

Kristian Svennevig [a,*], Marie Keiding [a], Niels Jákup Korsgaard [a], Antoine Lucas [c], Matthew Owen [a,e], Majken Djurhuus Poulsen [b], Janina Priebe [f], Erik Vest Sørensen [a], Costanza Morino [d]

[a] GEUS, Geological Survey of Denmark and Greenland, Copenhagen, Denmark
[b] GEUS Nuuk office, Nuuk, Greenland
[c] Université Paris Cité, Institut de physique du globe de Paris, CNRS, France
[d] CNRS - Laboratoire Environnements, Dynamiques et Territoires de la Montagne, Université Savoie Mont Blanc, UMR 5204, Chambery, France
[e] MarineSpace Ltd, Norwich, United Kingdom
[f] Department of Historical, Philosophical and Religious Studies, Umeå University, Umeå, Sweden

HIGHLIGHTS

- The hitherto undescribed 1952 Niiortuut landslide-tsunami disaster in Greenland can be attributed to permafrost degradation.
- This is the earliest recorded historical disastrous permafrost degradation landslide in the arctic.
- As Arctic slopes continue to warm, we can expect this type of landslide activity to increase even more.
- As such the Niiortuut landslide may serve as a model for future hazard scenarios.

GRAPHICAL ABSTRACT

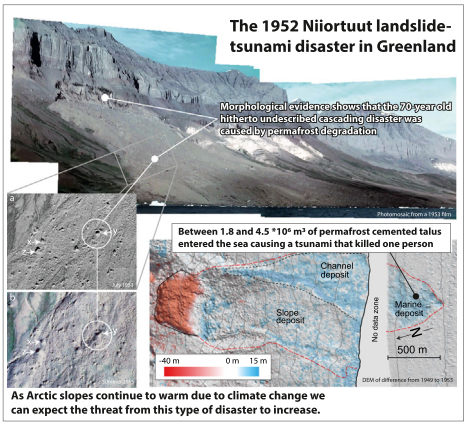

ARTICLE INFO

Editor: Jay Gan

Keywords:
Landslide
Arctic
Tsunami
Disaster
Permafrost degradation

ABSTRACT

On December 15th 1952, at approximately 14:00 local time a mass of 5.9 × 10^6 m^3 of permafrozen talus deposits failed in a landslide close to the Niiortuut mountain on the south coast of the Nuussuaq peninsula, central West Greenland. Between 1.8 and 4.5 × 10^6 m^3 of the material entered the sea and generated a tsunami that propagated through the Vaigat strait (*Sullorsuaq*). Here we describe this catastrophic event for the first time by analysis of historical material supplemented by recent fieldwork and discuss the implications for the state of contemporary permafrozen slopes. The tsunami killed a fisherman working on the shore of southern Nuussuaq, 10 km south-east of the landslide. In the mining town of Qullissat, 30 km south of the landslide, it had a runup height of 2.2–2.7 m and caused minor material damage. Morphological evidence show that the basal surface of rupture was 80 m inside the permafrost cemented talus slope, whose degradation was a dynamic conditioning factor for the landslide. The 1952 Niiortuut landslide is the first historically recorded event of permafrost degradation induced landslide-tsunamis in the Arctic. We infer that the landslide and its cascading consequences occurred due to the early-twentieth century warming that started in the late 1910's in the Arctic. Warming is now increasingly affecting this region, as shown by an enhanced recent landslide activity.

* Corresponding author.
E-mail address: ksv@geus.dk (K. Svennevig).

http://dx.doi.org/10.1016/j.scitotenv.2022.160110
Received 28 September 2022; Received in revised form 4 November 2022; Accepted 6 November 2022
Available online 9 November 2022

1. Introduction

With the current warming climate, the frequency and magnitude of landslide events in the Arctic are expected to increase due to changes in precipitation, permafrost degradation and glacial retreat (Gariano and Guzzetti, 2016; IPCC, 2019; Patton et al., 2019; Sæmundsson et al., 2021). Landslide-tsunamis are among the most devastating consequences of this, as demonstrated by recent events in Greenland (Dahl-Jensen et al., 2004; Paris et al., 2019; Svennevig et al., 2020, 2022), Alaska (Higman et al., 2018) and Chile (Sepulveda et al., 2010). But how far back in historical time can we trace such climate-change dependent landslides in the Arctic?

The study of historic landslide-tsunamis in the Arctic is crucial to understand the risk of similar events occurring in the future. However, due to the sparse population and the remoteness of these territories, the frequency and magnitude of these events are largely unknown. This is also the case for Greenland, where only three tsunamigenic landslides from 1952, 2000 and 2017 have ever been recorded (Svennevig, 2019), of which only the two most recent ones have been studied in detail (Dahl-Jensen et al., 2004; Svennevig et al., 2020).

Here, we describe for the first time the 1952 Niiortuut landslide and related tsunami. We investigate the morphological and geological conditions and settings of this earliest historically recorded tsunamigenic landslide in Greenland, focussing on the degrading state of permafrost as a dynamic conditioning factor for the landslide.

1.1. State of the art

We follow the landslide terminology of Hungr et al. (2014). As the landslide is not straightforward to classify, we keep the broad term "landslide" for the descriptive part of the paper and interpret the specific type of landslide in the Discussion section.

Very little is known about the circumstances of the December 15th, 1952, Niiortuut landslide and tsunami. The landslide was firstly named by Svennevig (2019) after the nearby Niiortuut mountain, 3 km to the north-west. The event was briefly mentioned in several contemporary newspaper articles (see Materials and Methods), but it has been scarcely reported in the scientific literature. The landslide was firstly outlined – but not described – on a 1:100,000 scale geological map (Rosenkrantz et al., 1976). Pedersen et al. (2002) and Dahl-Jensen et al. (2004) in their works on the nearby 90 × 10^6 m^3 November 2000 Paatuut rock avalanche briefly mention the Niiortuut event (as "a 1952 landslide"). The authors identify the area of West Greenland from Svartenhuk Halvø to Disko Island *(Qeqertarsuaq)* – where basalts overly sediments of the Nuussuaq basin – as at risk of tsunamigenic landslides, with the south-facing slope of Nuussuaq (Fig. 1) being considered an area of especially high risk. On this slope, Benjamin et al. (2018) mapped 20 rock avalanche deposits to calibrate a numerical flow model, including the Niiortuut landslide. Numerous other landslide deposits are identified in the 1:100,000 scale geological mapping of Disko and Nuussuaq (Pedersen et al., 2001, 2007), and Svennevig (2019) reports that two thirds of the post glacial landslides in Greenland are located in the geological province of the Nuussuaq Basin. Recently, in June 2021, a landslide of about 20 × 10^6 m^3 occurred 7 km south-east of the Niiortuut landslide, without producing a tsunami (Fig. 1a). Svennevig et al. (2022) named this the Assapaat frozen debris avalanche and suggested the dynamic conditioning factor to be permafrost degradation.

Greenland is affected by landslides outside the Nuussuaq Basin too. The Karrat Landslide Complex, 150 km north of Niiortuut, has been recently affected by three large rock avalanches in 2009, 2016 and 2017 (Svennevig et al., 2020), the latter producing a devastating tsunami that killed four people in the nearby village of Nuugaatsiaq (Paris et al., 2019) and had a devastating effect on the coastal landscape here (Strzelecki and Jaskólski, 2020). Svennevig et al. (2020) discovered three continuously active areas in the Karrat Landslide Complex that still pose a potential threat to local communities in the fjord system.

1.2. Research targets

The 1952 Niiortuut landslide is the earliest known historical landslide in Greenland (Dahl-Jensen et al., 2004, Svennevig, 2019). As such, it is an important example that can contribute to the understanding of the development of landslides and related future hazard in the Arctic. The aim of this paper is two-fold: 1) to describe a unique case of a tsunamigenic landslide for the first time with an unprecedented and never-analysed dataset composed of a variety of historical sources along with recent primary data; 2) to discuss the implications of this oldest-known historic landslide in this region in the context of a warming Arctic climate.

1.3. Geographic and geological settings of the study area

The study area is located in central West Greenland (70°21′3"N, 53°10′23"W) on the south coast of the Nuussuaq peninsula facing the Vaigat strait (*Sullorsuaq*) (Fig. 1a). The topography is shaped by repeated Quaternary glaciations creating coastal slopes up to 2000 m high along the up to 600 m deep, 15 km wide and 100 km long Vaigat strait. The strait was deglaciated between 12 and 10 ka BP (Weidick and Bennike, 2007), and has since experienced c. 80 m of isostatic rebound (Weidick, 1992).

The present climate is polar, and the slopes in the region are modelled to host discontinuous to continuous permafrost (Westergaard-Nielsen et al., 2018). The mean annual air temperature is −8.4 °C in Saqqaq, a settlement located at sea level 60 km to the south-east of the landslide area (Fig. 1a). West Greenland represents an area of tectonic stability and only few minor tectonic earthquakes are known (Voss et al., 2007).

The bedrock geology of the coastal slopes of the Vaigat strait consists of Cretaceous-Paleocene sediments of the Nuussuaq Group overlain by extensive Palaeogene volcanic rocks and intruded by associated sills and dykes (Henriksen et al., 2009) (Fig. 1a). At the site of the landslide, mudstones and poorly lithified sandstones of the Albian-Paleocene of Nuussuaq Group (Dam et al., 2009) form the bedrock of the coastal slope up to 600 m elevation, where they are overlain by an up to 900 m high cliff comprising the Paleocene Vaigat and Maligât Formations of hyaloclastite breccias and subaerial lava flows capped by basalts (Pedersen et al., 2017, 2018). A topographic ledge is located along most of the coast between the subvertical hyaloclastite cliff and the sediments. This ledge is covered by colluvium and is capped by thick actively forming talus deposits derived from the volcanic rocks (mainly hyaloclastite) of the Vaigat and Maligât Formations. These talus deposits are present at 500 m elevation on both sides of the Niiortuut landslide scarp, where they form talus slopes up to 200 m high.

In 1952, the nearest settlement to the landslide was the coalmining town of Qullissat, located 30 km to the south, on the northern coast of Disko Island on the opposite side of Vaigat strait (Fig. 1a). With a population of 995, it was the third-largest settlement in Greenland at that time, and a cultural hub. The mine was closed in 1972, after mining operations had become less profitable, and the inhabitants were resettled, and the town abandoned. In November 2000, the low-lying parts of Qullissat were destroyed by the tsunami resulting from the Paatuut rock avalanche, which had an estimated volume of 90 × 10^6 m^3 (Pedersen et al., 2002; Dahl-Jensen et al., 2004).

2. Materials and methods

To investigate the landslide we have used: 1) historical nadir and oblique photos to examine the landslide before and after the event; 2) differential digital elevation model (DEM) produced from these images to constrain the volume mobilized during the event; 3) multibeam bathymetry data to examine the morphology and volume of the material that entered the sea and caused the tsunami; 4) field observations; 5) historical reports and interviews with eyewitnesses to better constrain the event; 6) morphometric analysis of the generated DEMs.

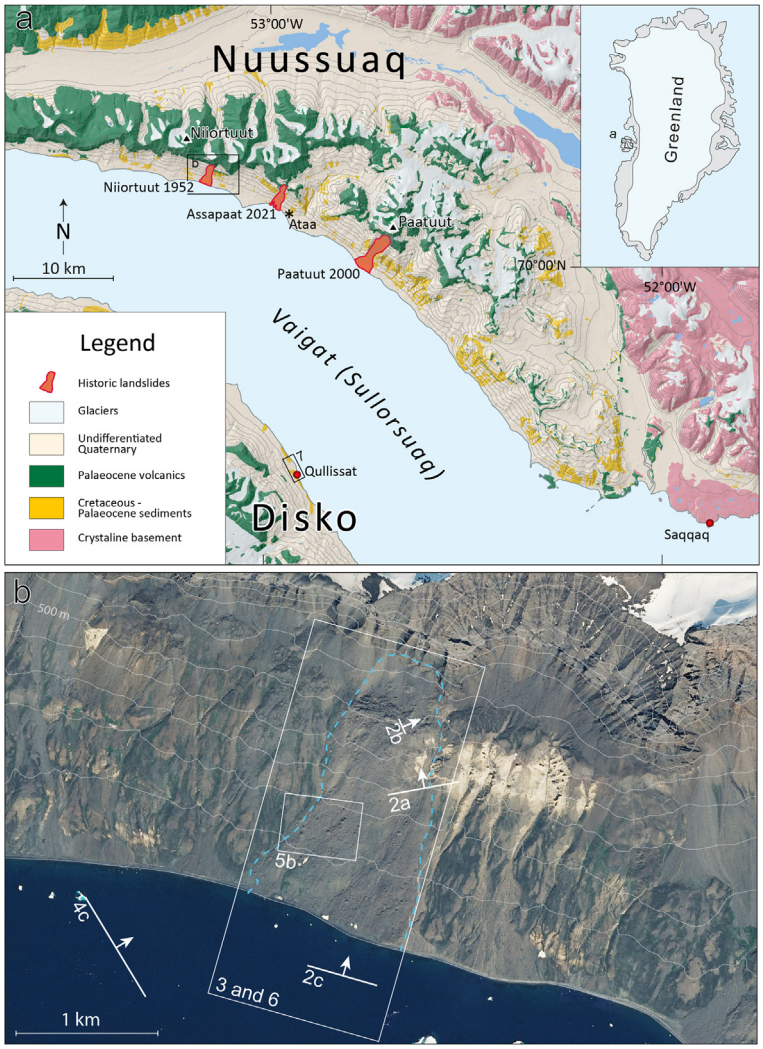

Fig. 1. a) Simplified geological map of the Vaigat area based on the 1:100000 scale geological maps from GEUS (Rosenkrantz et al., 1976; Pedersen et al., 2001, 2007). Historical landslides are shown along with place names mentioned in the text and position of Fig. 1b and Fig. 7. The estimated position af where the fisherman died is shown with a * at Ataa. b) orthofoto of the area of the landslide from the Danish Agency for Data Supply and Infrastructure (SDFI) from 2016. The onshore part of the landslide is shown with stipled blue outline. The positions of photos in Figs. 2 and 5 are shown along with the detailed maps in Figs. 3 and 6.

2.1. Photos, film and digital elevation models (DEMs)

We use a variety of historic and recent photographic datasets to characterise the geomorphology and dynamics of the landslide. A series of overlapping oblique aerial photos recorded on 24th July 1949 by the Danish Geodetic Institute (today the Danish Agency for Data Supply and Infrastructure, SDFI) represents the only functioning dataset of the area before the Niiortuut landslide, apart from a similar, but poorly preserved, dataset from 1948. We used the 1949 images to produce a 5 m DEM of the area prior to the landslide, and to evaluate the pre-slide setting of the slope.

We used nadir aerial photos at 1:45,000 scale recorded in July of 1953 by the US Navy, half a year after the landslide occurred, to produce another 5 m DEM. We subtracted this from the DEM produced from the 1949 images to produce a DEM of Difference (DoD) to constrain the onshore volume changes caused by the landslide.

A 2 min 40 s long 16 mm colour film clip was recorded at the site of the landslide in the summer 1953. The clip is part of a longer film recorded during one of the "Nuussuaq expeditions", a series of scientific expeditions to the Nuussuaq peninsula from 1938 to 1968 lead by Professor A. J. Rosenkrantz. In old field notes we found that the clip was recorded from boat on 26th July 1953, seven months after the event. This data is used in Figs. 4 and 5 to show the conditions at the landslide half a year after it occurred. The field notes also report that at least six colour photos were taken during the expedition, but unfortunately, we have not been able to recover these.

During July 2019, we performed fieldwork to examine the landslide for the first time. We acquired helicopter-based oblique aerials to produce a 0.15 m orthophoto and DEM that we used to perform morphometric analyses, which included the characterisation of the molards (sensu Morino et al., 2019) on the landslide deposits. Because some gaps were present in the derived DEM and orthophotos for the sub-horizontal area below the scarp, molards in this area were mapped using 1 m orthophotos from 2016 from SDFI. Molards were mapped when visible at 1:300 scale. Those that were not obviously distinguishable or for which there were no elevation data due to distortion in oblique photogrammetry were discarded.

2.2. Bathymetry data

Multibeam bathymetry data was acquired in Vaigat strait during a cruise using the vessel *Sanna* in September 2019. A subset of the data, that covers the submarine deposit of the landslide, was used to constrain the geometry and volume of the terminal lobe of the deposits. As the coastal waters in this part of Greenland are largely uncharted, and there was a

significant presence of ice, it was not possible for the survey vessel to go closer than 200 m from the shore at a water depth of about 40 m. Around the terminal lobe of the landslide, the multibeam has been processed to a DEM with a spatial resolution of 5 m. We reconstructed the pre-slide bathymetry by masking out the landslide affected area out of the DEM and replacing it with a new DEM interpolated from contour lines from the surrounding seabed. Subtracting this interpolated seabed from the bathymetry derived DEM resulted in a synthetic DoD for the submarine part of the landslide.

2.3. Historical records

Historical sources (other than the photographic datasets mentioned above) include contemporary newspaper articles, and interviews with eyewitnesses.

A key historical record is an article in Greenlandic with the title "Nûgssuarme kákap sisôrnerssua, inûp inûneranik nalekarpo" ("Large landslide costs lives"), published in February 1953 in *Avangnâmiok* ("The North Greenlander"), a monthly periodical distributed primarily in the central western and northern part of Greenland. The description of the event is based on various eyewitness accounts recorded soon after the event. This is the only detailed contemporary written account of the event, and it gives a brief description of the area of the landslide just after the event, along with descriptions of the impact of the tsunami in Qullissat and on the south coast of Nuussuaq. The local newspaper of Qullissat, *Kutdlek*, was first published after the event in October 1953, and did not have any references to the landslide or tsunami.

Another valuable source is the interview conducted by KNR (Kalaallit Nunaata Radioa, Greenland's national radio) with Frederik (Fari) Mathiassen in November 2000 in the wake of the November 2000 Paatuut rock avalanche and tsunami. Fari witnessed the 1952 tsunami while being in Qullissat and gives detailed accounts (in Greenlandic) of the event. Fari was also interviewed over the phone in brief by a researcher from GEUS in 2001 about the event.

We have also interviewed then resident of Qullissat Hans Anthon Lynge in May 2019. At the time of the event, in 1952, he was seven years old and recounts how the waves were observed in Qullissat. He reports that to his knowledge he is the last eyewitness to the event still alive.

We analysed several news items that were published two to three days after the landslide in Danish national and regional newspapers, on the 17th and 18th of December 1952. The articles are all similar and have the same source of information, namely RB, which probably is Ritzaus Bureau, a Danish news agency.

We have not found any mention of the event in any documents of public authorities, as archival research in the Danish National Archives did not return relevant results. This might be because the administrative system was reorganized during the 1950s and documents might have been placed in other directories or simply lost.

3. Results

There is little contemporary information on the landslide, the deposits and features of which remain clearly visible on the slope, while there are some historical accounts of the tsunami, but no physical remnant of the resulting damages is preserved. For this reason, in the Results section, we first describe the landslide as it appears today in the landscape. Then we expand on this description with historical data on the landslide, and finally with historical sources on the tsunami event.

3.1. The landslide

3.1.1. Morphological observations

The total length of the landslide (L) from the scarp to the outermost deposit is 2750 m and the height (H) 800 m, resulting in a H/L of 0.29 and a *Fahrböschung* angle of 16.2°.

3.1.1.1. Source area. The source area of the landslide is in the talus slope below a 60° steep hyaloclastite cliff, at 500 to 700 m elevation, which today is visible as a 650 m by 450 m scar (Fig. 2a). The backscarp is 60 m high, dipping 60° to the south, and extends to and coincides with the cliff face above the talus slope, showing that the landslide was released along the bedrock/talus slope interface. Three, approximately 20 m wide relict talus cones of the pre-slide talus slope are perched against the cliff face (marked with the green arrows in Fig. 2a). Since the landslide occurred, a new talus slope has developed within the source area. The lower part of

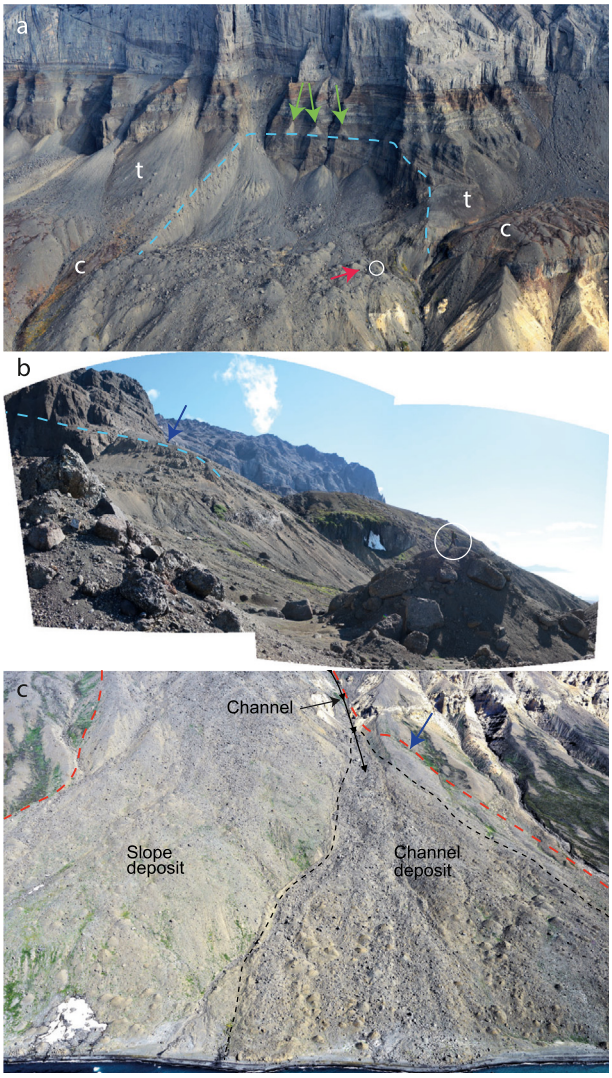

Fig. 2. Field photographs from 2019 a) Oblique aerial photo of the source area in the talus slope below the grey/brown cliff of Paleocene hyaloclastite and above the light-yellow Cretaceous sediments. Talus and colluvium on the surrounding slope are showed with t and c respectively. The stippled blue line outlines the backscarp and the green arrows shows the top of the relict talus slope, the lower part of which was involved in the landslide. The red arrow shows the position and direction of the photo in Fig. 2b and the white circle highlights the molard with the person on top in Fig. 2b. b) mosaic of two field photos showing observations near the source area of the landslide. The backscarp is shown with a stippled blue line and the blue arrow indicates where it breached the talus slope. In the foreground are two molards comprising the same material as the talus slope. Person for scale on top of molard is shown with a white circle. c) oblique aerial photo of the lower 400 m of the slope with the landslide outline shown with stippled red line and the main morphological zones; channel, channel deposit and slope deposit shown. The channel deposit is shown with stippled black outline and the blue arrow shows where the landslide overflowed the channel. See Fig. 1b for position of photos.

the sliding surface is covered by this new talus slope and landslide deposits with a 7° slope.

3.1.1.2. Depositional area. The landslide deposits consist exclusively of mobilized talus and colluvium. The onshore depositional area is 1800 m long and up to 1200 m wide in its terminal sector. At least 839 conical mounds consisting of landslide debris are pervasively scattered on the hummocky landslide surface (Figs. 2 and 3). They range from 7 to 590 m^2 in area, with an average area of c. 22 m^2. Their height ranges from a few decimetres up to 9 m high, with an average height of c. 2.5 m. They are mostly concentrated in the onshore terminal part of the landslide (Figs. 2c and 3). These are termed molards and are inferred to have been formed by the thawing of permafrozen ice cemented blocks of talus and colluvium (Morino et al., 2019), see further evidence of this in paragraph 3.1.2.1 on historical records of the landslide.

The onshore depositional area is divided into two different zones based on geomorphological characteristics (Fig. 3): 1) a south-eastern channel depositional zone characterised by an average slope of 20° and 603 molards scattered on its surface (Fig. 3). It is situated below an up to 40 m deep channel in the south-eastern part of the landslide, at 300 m elevation; 2) a south-western slope depositional zone with an upper average slope of 11° and a lower of 23° and covered by 236 molards. In the westernmost part of this zone, a subordinate lobe has stopped 100 m from the shore (marked with a x in Fig. 3).

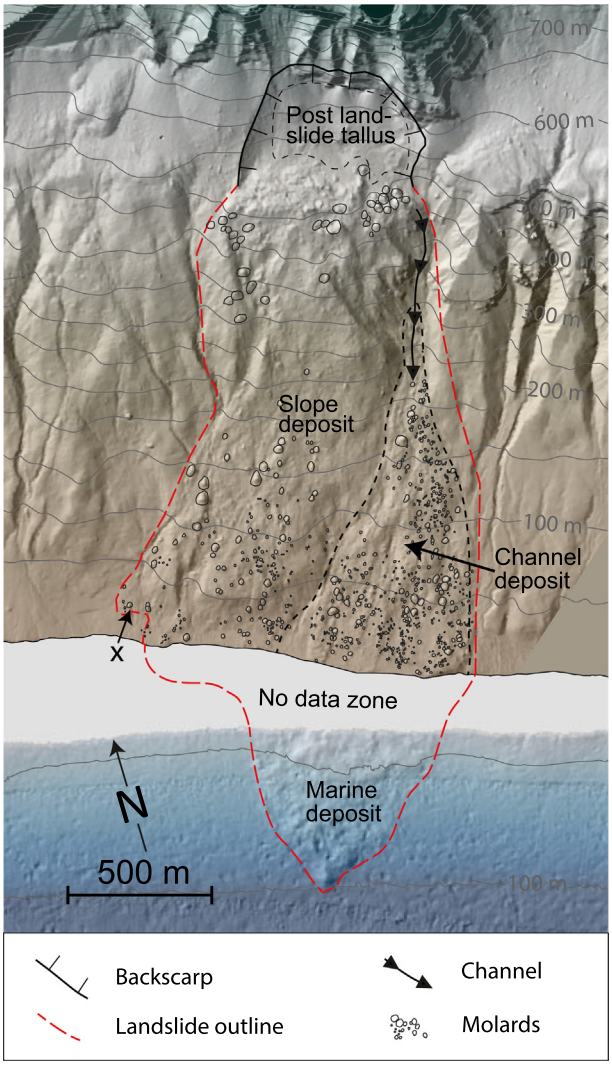

Fig. 3. Morphological map of the Niiortuut landslide area. Based on field observations and a DEM produced from 2019 oblique aerials. Molards (See Fig. 5), deposit zones and other significant morphological features are shown. X marks a subordinate lobe where the landslide did not reach the sea.

The channel depositional zone has almost three times more molards than the south-western slope depositional zone within a three times smaller area, given that the area of the channel depositional zone is 0.4 × 10^6 m^2, while it is 1 × 10^6 m^2 for the south-western slope depositional zone. The south-western slope depositional zone is recolonized by vegetation, which is largely absent on the channel depositional zone (Fig. 2c).

Part of the landslide body was emplaced in the sea immediately offshore the channel depositional zone, and the most distal submarine deposits are visible in the bathymetry data. Here the landslide terminal lobe is 600 m wide, 520 m long and up to 15 m thick and has a hummocky morphology like that of the onshore channel deposit zone (Fig. 3). The largest hummock is in the most distal part of the deposits, protrudes 12 m from the seabed, and has an area of 4000 m^2.

3.1.2. Historical records of the landslide

The historical accounts of the landslide are limited. Danish contemporary newspapers on December 17th and 18th 1952 all recount the same short news telegram, describing a loud noise ("an explosion"), a dust cloud, and estimating the area of the landslide to be four square kilometres. In the article in *Avangnâmiok* there is a short description of some locals visiting the site the day after the landslide. They describe how "immeasurably large amounts of rocks had been loaded into the sea". Cracks were still visible through the snow cover in the source area, and it was noted that the landslide was very dry around the streams coming down the slope. Finally, the witnesses report that they were surprised that the landslide was not larger compared to the size of the waves they had observed.

3.1.2.1. Historical photos

3.1.2.1.1. From before the landslide. Analysis of the oblique aerial photos from 24th July 1949 – three-and-a-half year prior to the landslide – shows a light lineament, which is an incipient backscarp in the talus slope below the 60° steep cliff (Fig. 4a). In the field, we have observed similar structures in several talus slopes on the south coast of Nuussuaq. The light lineament is 9 to 22 m long (downslope). The upper part of the slope, from 650 to 200 m had a pre slide gradient of 30° and the lower 200 m a gradient of about 15°.

3.1.2.1.2. From after the landslide. The two sets of images from July 1953, seven months after the landslide, allow us to analyse the landslide dynamics. The 1:45000 scale aerial photos show that the lineament observed in the 1949 photos developed into the scarp (Fig. 4b). The 1953 aerial photographs and the 16 mm colour film show a dark staining in the backscarp (Fig. 4b, c). Both the 1953 aerial photographs and the 16 mm colour film show angular blocks on the landslide deposit (Fig. 5a, c) that in the 2016 orthophoto have developed into conical hummocks (Fig. 5b) confirming that these are permafrost molards.

3.1.3. DEM of difference (DoD) and volume estimates

3.1.3.1. Onshore volumes. We produced a DoD from the 1949 DEM and the 1953 DEM to constrain the onshore volume changes caused by the landslide event (Table 1 and Fig. 6). In doing so we assume that the landslide occurred in one single event and that the DoD spanning the 3.5 years records the volume that entered the sea on December 15th, 1952 and caused the tsunami. The DoD shows that erosion was confined to the scarp area and that the net onshore depositional area is from 500 m elevation down to the coast. The two onshore depositional areas described on the morphological map (Fig. 3, channel deposit zone, slope deposit zone) are marked on the DoD.

The volume of the eroded area in the scarp (V_{Scarp}) is calculated as 5.9 × 10^6 m^3. This number is to be taken as a minimum, as part of the deposits are perched in the source area. The basal surface of rupture reached 80 m inside the talus cone. The slope zone is covered by a thin veneer of landslide deposit that in places is close to the detection limit of the DoD (Fig. 6). Locally, in two places just outside the scarp and in the most western part near the shore, the landslide deposit is up to 20 m thick. This consists of 1.3 ×

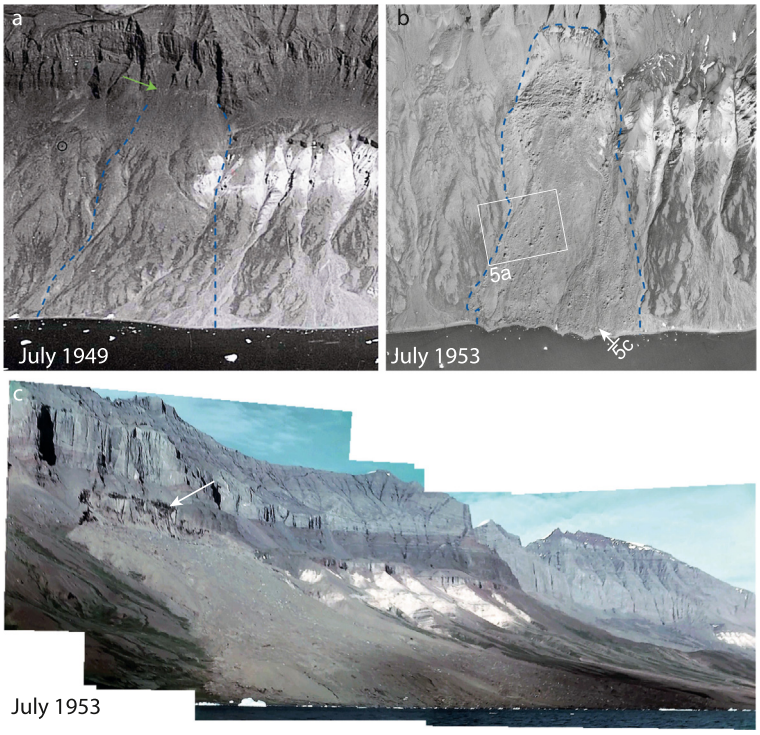

Fig. 4. Historical images. a) Extract of oblique aerial photograph recorded in July 1949 showing the coastal slope 3½ year before the landslide. Notice the light grey lineament at the top of the talus slope (green arrow) coinciding with the top of the future 1952 Niiortuut landslide. The lateral extent of the landslide is shown with blue stippled lines. b) Extract of a July 1953 1:45000 scale aerial image (not orthorectified) from ½ a year after the landslide. Outline of the landslide is indicated with blue stippled line. Positions of photos in Fig. 5 is shown. c) Photomosaic compiled of frames from a 16 mm colour film recorded on July 29th, 1953. Notice the dark colouration in the backscarp indicated with a white arrow. Viewing direction is towards the north-east. See Fig. 1b for position.

10^6 m^3 of material (V_{Slope}). The deposit in the channel zone is around 15 m thick but locally up to 27 m. It comprises 1.6 × 10^6 m^3 ($V_{Channel}$). Adding the volumes of the two zones gives a total onshore deposit volume ($V_{Onshore}$) of 2.9 × 10^6 m^3 of material.

To compare the volumes eroded to the volumes deposited, a bulking factor of 1.25 was applied to the eroded volume in the scarp area (V_{Scarp}) to account for a volume increase of 25 % due to fragmentation during transportation. This is similar to the bulking factor suggested by Hungr and Evans (2004) and commonly used for rock avalanches (e.g. Schleier et al., 2015; Oppikofer et al., 2017). This amounts to a volume ($V_{Scarp\ bulk.}$) of the landslide of 7.4 × 10^6 m^3. Any 'missing' terrestrial volume in this budget is taken as the volume that entered the sea. Thus, subtracting $V_{Scarp\ bulk.}$ From the volumes deposited onshore ($V_{Onshore}$) gives an estimate of the material deposited at sea ($V_{Marine\ estimate}$) equal to 4.5 × 10^6 m^3. This is to be taken as a maximum volume estimate.

During the landslide the coast advanced up to 90 m creating 47,000 m^2 new land (green polygon, Fig. 6) observed in the 1953 aerial photographs. Today much of this area is eroded. As pre landslide bathymetry is not available, the volume in this area (green polygon Fig. 6) is not accounted for in our volume budget.

3.1.3.2. Submarine volume. The area of the marine deposit of the landslide covered by the bathymetrical survey is 22,000 m^2 and the reconstructed volume of the deposits in this area ($V_{Marine\ mapped}$) is 0.90 × 10^6 m^3. We estimate the area of the deposit within the marine no data zone, north of the area of bathymetric data coverage to be 21,000 m^2 (Fig. 3). Assuming the thickness of the deposit here is the same per area as in the mapped submarine area gives us a volume of about 0.9 × 10^6 m^3 for the unmapped part of the deposit ($V_{Marine,\ calc.}$). The estimated total volume of material that entered the sea (V_{Marine}) is thus 1.8 × 10^6 m^3. This volume does not account for the landslide entraining seabed material or compacting the seabed deposits along its runout, so our estimate is a minimum.

3.1.3.3. Marine and onshore volume comparison. Comparing the marine volume (V_{Marine}, 1.8 × 10^6 m^3) calculated from the marine mapping and the estimated marine volume from the onshore mapping ($V_{Marine\ estimate}$, 4.5 × 10^6 m^3) gives a difference of 2.7 × 10^6 m^3. We suggest that this difference is most likely due to an underestimation of the volume in the no data zone ($V_{Marine,\ calc.}$), which may be expected to have a greater deposit thickness than the more distal area that is mapped. The fact that the coast advanced by up to 90 m shows that a significant volume of material could be present here. It is also possible that marine deposits will have experienced a greater rate of erosion than the terrestrial deposits due to the effect of waves and icebergs. Other factors affecting the volume budget is the bulking factor used or the fact that approximating the base of the marine deposit as an extension of the surrounding seabed is an oversimplification, thus underestimating the mapped marine volume (V_{Marine}). From the above we can conclude that between 1.8 × 10^6 m^3 and 4.5 × 10^6 m^3 of landslide material entered the sea.

3.2. The tsunami

Traces of the 1952 tsunami have been erased by general erosion and weathering as well as the larger tsunami after the Paatuut rock avalanche in 2000, which had a near field runup of 50 m (Dahl-Jensen et al., 2004), thus making historical records and eyewitnesses the only sources of information. The tsunami was observed in two places: in the town of Qullissat, 30 km south of the landslide, and near a trapper hut at Ataa, 10 km south-east of the landslide (Fig. 1a). Evidence of the tsunami inundation was observed near the landslide the following day by eyewitnesses. We could not observe traces of the tsunami inundation, such as damaged vegetation, in the black and white 1953 aerial images.

3.2.1. In Qullissat

According to the article in *Avangnâmiok*, the tsunami reached the town of Qullissat at around 14:00 local time on the 15th December 1952. In

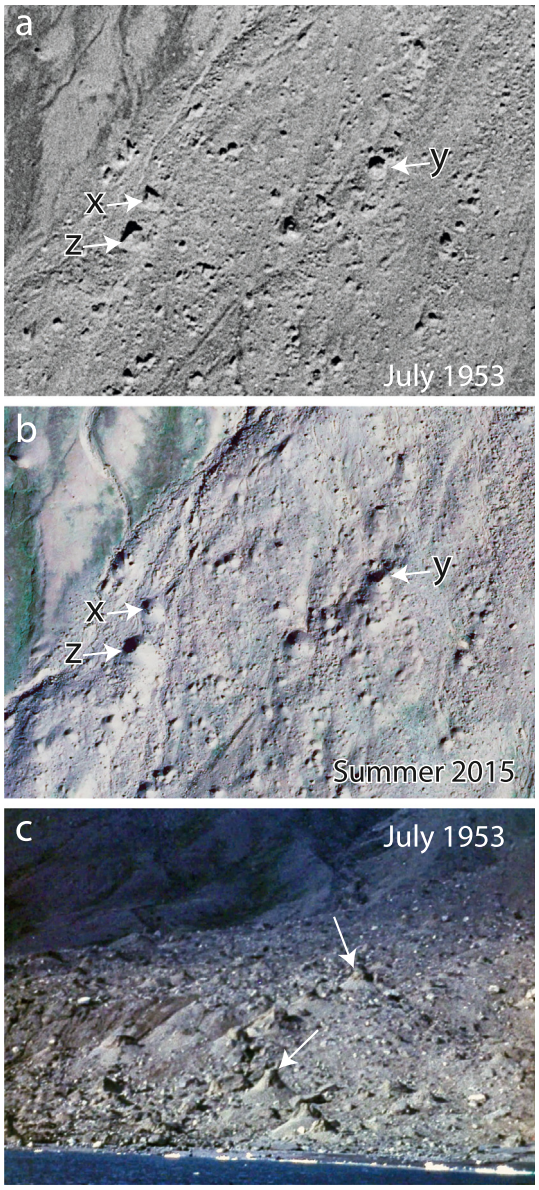

Fig. 5. Aerial photographs from 1953 (a) and 2016 (b) showing the same extent of the slope deposit. Notice how the angular blocks (some are marked x, y and z) in 1953, half a year after the landslide, today are degraded into hummocks (same marked x, y and z as in a) thus demonstrating that the hummocks are molards. The blocks marked x, y and z in the 1953 aerial are 30 m, 20 m and 40 m across respectively. See Figs. 1b and 4b for location. c) Extract of frame from a 16 mm colour film recorded July 29th, 1953 showing the lower part of the channel deposit zone. Notice the angular permafrozen blocks of talus/colluvium in the process of thawing and degrading into molards. Two of these are highlighted with white arrows. Viewing direction is towards north - north-west. See Figs. 1b and 4b for location.

Avangnâmiok, it is described that at this time, the tide was close to ebb, but not the lowest tide. We do not have the tidal values for Qullissat. The present day tidal range of Saqqaq, 40 km west of Qullissat, is −1.2 m to +1.5 m, however, the extreme values are only observed at neap tide according to tidal models (Ribergaard, 2022). According to the model, at 14:00 local time on the 15th December 1952 in Saqqaq the tide was at −0.2 m relative to mean sea level (msl) and increasing (Mads Hvid Ribergaard pers. comm). This is not in contrast to the article in *Avangnâmiok* and we assume that this value is applicable to the tide in Qullissat when the tsunami hit.

The recently acquired eyewitness account of, then seven-year-old, Hans Anthon Lynge observing the waves in the southern part of Qullissat enables us to estimate the runup elevation in this area to be 2–2.5 m and surpassing the high-water mark (presumably at 1.5 m above msl) (Fig. 7). Contemporary Danish newspapers report on a telegram (e.g., Børsen, 18 Dec 1952 "Fire Kvadratkilometer Land styrtet I havet ved Godthaab" which translates to "Four square kilometres of land have slid into the sea near Qeqertarsuaq") describing a maximum runup of 1.5–2 m, and a maximum inundation 30–40 m inland from the coast in Qullissat. It is unknown if this runup takes the low tide into account.

The tsunami's impact on the town of Qullissat is described in *Avangnâmiok*, based on eyewitness accounts of the driver Hans Møller, who was in his car on the way to the mine entrance south of town when the first wave hit (Fig. 7). According to Møller, the mass of water was enormous. The waves washed fish that seemed to be halibut up onto the road to the mine. These fish are usually found in deep water far from the coast. Møller mentioned that there were several waves, of which the third one was the largest, powerful enough to wash up ice and debris into his car. Records of the damages to the infrastructures in the community are limited. Eyewitness Frederik (Fari) Mathiassen says that no buildings were damaged following the event, but that water entered the power plant, located at 2 m elevation above msl in the southern part of the town (Fig. 7).

Table 1
Modelled and estimated volumes.

	Volume (10^6 m^3)	Note
V_{Scarp}	5.9	Eroded volume in the scarp, a minimum, as parts of the deposit is still inside the scarp.
$V_{Scarp\ bulk.}$	7.4	V_{Scarp} with applied bulking factor of 1.25
V_{Slope}	1.3	Volume of the slope deposit zone
$V_{Channel}$	1.6	Volume of the channel deposit zone
$V_{Onshore}$	2.9	V_{Slope} + $V_{Channel}$
$V_{Marine\ estimate}$	4.5	Difference ($V_{Scarp\ bulk.}$ - V_{Slope} + $V_{Channel}$)
$V_{Marine\ mapped}$	0.9	Mapped and calculated from the bathymetry
$V_{Marine,\ calc.}$	0.9	Calculated in no data zone
V_{Marine}	1.8	$V_{Marine\ mapped}$ + $V_{Marine,\ calc}$

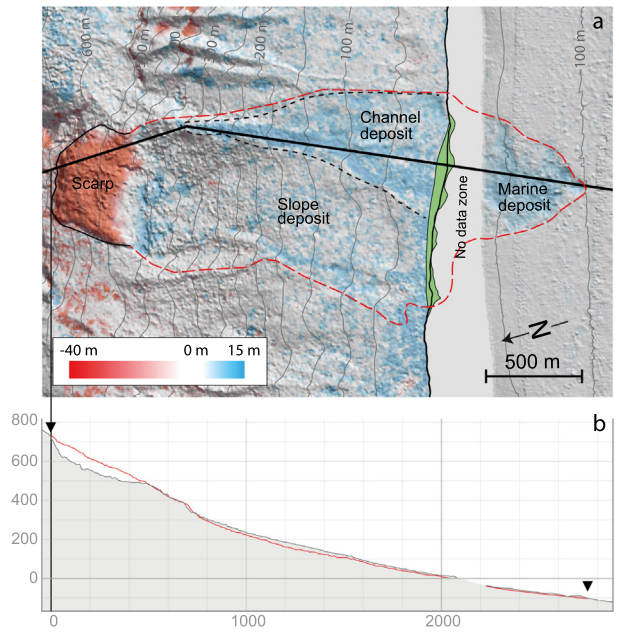

Fig. 6. a) DEM of Difference (DoD) of the Niiortuut landslide made from 1949 and 1953 DEM's from the onshore area and the recent bathymetrical mapping for the offshore area. The green polygon on the shore shows how much the coastline advanced during the landslide as observed in the 1953 aerial images. The hillshade overlay is from the 1953 DEM. b) Elevation profile through the scarp and the channel deposit of the landslide (along bold black line in a). The red line is the 1949 pre-landslide elevation and the dark grey with light grey filling is the 1953 post landslide elevation.

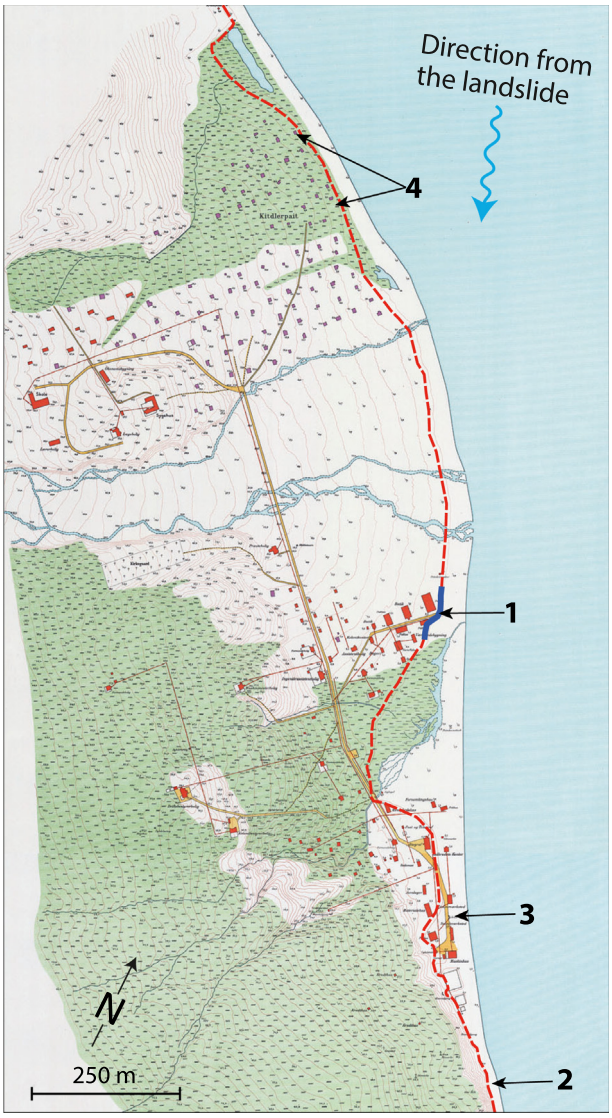

Fig. 7. Observed (blue) and inferred (red) runup marked along the 2.5 m contour from the 1952 Niiortuut landslide- tsunami in Qullissat. 1 shows the position of eyewitness Hans Anton Lynge, 2 the approximate position of the driver Hans Møller and 3 the position of the coal crane and power plant that was reported damaged during the tsunami. 4 marks the position of the lowermost houses in the northern part of the town that were presumably not inundated. The direction from the landslide is shown with a blue wavy arrow in the upper left corner. Background map is an extract of a topographical map of the town surveyed in 1948, published in 1950. Red polygons on the map are public buildings and purple are private houses. See Fig. 1a for location.

Unconfirmed word of mouth accounts mention that the concrete foundation of a coal crane at 1.7 m elevation above msl on the beach was damaged (Fig. 7).

Based on the above records we estimate that the tsunami runup was 2–2.5 m above msl in southern Qullissat. Compensating for the low tide of presumably −0.2 m gives a total runup height of 2.2–2.7 m here. We have not found any records of tsunami runups in northern Qullissat, where we would have expected a higher runup, as this section of the coast is more exposed towards the direction of the landslide (Fig. 7). The northern part of the town has exclusively private houses, which were located above 5 m elevation at the time of the event. The lowermost two houses were at 3.1 m and 3.5 m above msl respectively (marked 4 in Fig. 7). We can assume that here, the wave runup was lower than 3.1 m, as damage to these houses would presumably have been reported.

3.2.2. On Southern Nuussuaq

The article in *Avangnâmiok* reports the witness account of the surviving fishermen who were working on a barge with fishing nets on the south coast of Nuussuaq, 10 km south-east of the landslide, near Ataa (Fig. 1). On the day of the landslide, they were at sea fishing for "whitefish" (beluga whale) for the workers in the coalmine in Qullissat and had caught four. After fishing, they were cleaning their nets on the beach at southern Nuussuaq. The exact location of this is unknown, but as the survivors hiked to a travel hut, which is presumably at Ataa, we assume that the beach was close to this location, around 10 km south of the area of the landslide. At around 14:00 local time, they first saw what they thought was fog slowly dispersing at the site of the landslide and continued cleaning their nets. Then they saw a motorboat being pushed towards them by an iceberg carried by a large wave. The force of the wave lifted their pram to a vertical position in the water, and three of them were thrown up on land above the usual hightide mark. The fourth fisherman was killed in this event and his body was not found until the next day. The three survivors suffered injuries from ice blocks hitting them with the first wave but reached higher ground before a second wave hit the coast. After this they walked in their soaked and frozen clothes (air temperature was reportedly below freezing) to the travel hut at Ataa (Fig. 1), where they lit a fire and signalled for help with flares and were later rescued by a search party from Qullissat. In addition to the information on the events near Ataa, the article in *Avangnâmiok* reports the description from an eyewitness on how a group of people visited the site of the landslide the day after the event and how the waves had flooded a small nearby promontory, ripping up the grass and leaving icebergs above the high-water mark.

4. Discussion

Our compilation of data reveals the circumstances of the hitherto undescribed Niiortuut landslide-tsunami event in central West Greenland 70 years ago. The very limited direct observations of the slope prior to failure, the passage of time obscuring field evidence and mislaid archival material makes it difficult to characterise the event further, especially regarding conditioning and triggering factors. We can, however, reconstruct the following.

4.1. Summary of events

4.1.1. Before the landslide

Two and a half year prior to the landslide a 9 to 22 m high light lineament was visible at the top of the talus slope (Fig. 4a) coinciding with the backscarp in the 1953 aerial images. This lineament could be due to the tumbling of rocks along the scarp during progressive movement of the talus slope, exposing deeper talus not coloured by lichen growth and weathering. The lineament shows that the slope had started to move in 1949. How long this movement had been ongoing is difficult to say. From the recent Assapaat frozen debris avalanche (Svennevig et al., 2022), we know that the area that failed moved by c. 1 m/year measured by InSAR (Interferometric Synthetic-Aperture Radar) prior to the landslide. Applying this velocity to the 9–22 m high light lineament visible on the slope at Niiortuut in 1949 gives a rough age of <9–22 years of the movement at this point in time. This observation and lack of other morphological evidence (visible cracks, minor failures) in the images from 1949 lead us to infer that incipient movements prior to the landslide occurred no further back in time than a couple of decades.

4.1.2. The landslide

Our interpretation of the initiation and evolution of the landslide are based on field morphological observations and measurements (Figs. 2 and 3) and the historic photographic data (Figs. 4, 5 and 6). The landslide started at around 14:00 local time on December 15th, 1952 at 500 to 700 m elevation, where 5.9×10^6 m^3 of ice-cemented talus failed. The sliding surface was 80 m deep-inside the talus slope. We infer that the talus slope in the source area was permafrost cemented prior to failure because

molards are observed throughout the deposits (Fig. 3), and the scarp in the 1953 photos shows a dark colour (Fig. 4c) that can be interpreted as exposed thawing ground ice. Analogue observations have been made for the nearby June 2021 Assapaat frozen debris avalanche (Svennevig et al., 2022). We will discuss this further in the paragraph on the potential conditioning and triggering factor below.

After the release of material from the source area, 1.3×10^6 m^3 was deposited on the slope forming a thin veneer. The easternmost part of the landslide body entered a pre-existing gully and was channelized towards the sea (Figs. 3 and 4a). The evidence of the landslide overflowing the channel (blue arrow in Fig. 2c) suggests that in the upper part of the channel the landslide mass was at least 40 m thick. Onshore in this channel 1.6×10^6 m^3 of material was deposited. Between 1.8×10^6 m^3 and 4.5×10^6 m^3 of material entered the sea and caused the tsunami.

4.1.3. The tsunami

We have presented detailed accounts of the first-recorded historical landslide-tsunami and fatality from such an event in Greenland. Although the tsunami was relatively small (2–2.5 m runup in Qullissat, 30 km away) we note that, had the landslide happened at neap high tide (+ 1.51 m), the runup may have been about 2 m higher.

We have verified the volume and the runup recorded using the empirical relations described in the SPLASH formula (Oppikofer et al., 2018). The formula is based on empirical relations between landslide volume, distance from tsunami source and runup height from a database of eight rock avalanches in fjord settings. The estimated volume of the marine deposit is between 1.8×10^6 m^3 and 4.5×10^6 m^3 the distance to Qullissat of 30 km gives a calculated runup of 2.0 to 3.5 m. This agrees with the 2–2.5 m value estimated from historical datasets suggest that a volume estimate in the lower end of the 1.8×10^6 m^3 to 4.5×10^6 m^3 span may be more likely. Performing the same calculation for the village of Saqqaq (distance 60 km with a 40° bend of the wave path to account for the curvature of Vaigat, (Fig. 1a)) provides a runup of 1.0 to 1.8 m, suggesting that waves could have been observable here. We have not encountered sources reporting waves in Saqqaq after the 1952 Niiortuut landslide. According to the SPLASH formula the runup at Ataa, 10 km from the landslide assumed to be the place where the fisherman died, was between 4.5 m and 7.7 m high.

4.2. Classification of the landslide

The brief previous mentions of the Niiortuut landslide describe it as a generic landslide (Pedersen et al., 2002; Dahl-Jensen et al., 2004) or as a rock avalanche (Svennevig, 2019). The landslide initiated as a talus/debris slide and moved down the slope as a granular flow of blocks up to 40 m across (Fig. 5a), with high energy as indicated by the fact that it caused a tsunami. This is indicative of a rock avalanche (Hermanns et al., 2021; Hungr et al., 2014). However, the source material was not constituted of bedrock, but of talus (debris) deposits cemented by perennial ground-ice, and as such, we term the landslide a frozen debris avalanche, but stress that the landslide had the physical properties of a rock avalanche. This type of landslide was first introduced by Svennevig et al. (2022) for the Assapaat frozen debris avalanche, who inferred that this type of mass movements have the physical properties of a rock avalanche while moving downslope.

4.3. Comparison between the 1952 Niiortuut and the 2021 Assapaat frozen debris avalanches

There are several similarities between the 1952 Niiortuut frozen debris avalanche and the recent June 2021 Assapaat frozen debris avalanche, which is located 7 km south-east along the coast to the Niiortuut site (Fig. 1a). For the detailed description of this debris avalanche, please see Svennevig et al. (2022). Similarities include the shared geological setting, source material (comprising exclusively permafrozen colluvium and talus), similar scarp volume (5.9×10^6 m^3 vs 6.9×10^6 m^3) and elevation (700 m vs 850 m), and a similar slope gradient (30° in the upper reaches, and 15° in the lower). The deposits are also similar, in that they are dominated by molards, resulting from degradation of blocks of permafrozen talus and colluvium.

There are, however, four notable differences between the two landslides: 1) Concentric ridges and levees are observed in the distal part of the Assapaat frozen debris avalanche, whereas the Niiortuut frozen debris avalanche has no such ridges; 2) the presence of a pre-existing gully/channel on the slope of the Niiortuut frozen debris avalanche, while no pre-existing morphology affected the deposition of the Assapaat frozen debris avalanche; 3) the Assapaat frozen debris avalanche entrained a large volume of permafrozen soil/colluvium halfway down the slope (entrainment ratio (ER) between 2.5 and 3.8). No such entrainment is observed in the Niiortuut frozen debris avalanche. 4) 1.8×10^6 to 4.5×10^6 m^3 of the Niiortuut frozen debris avalanche entered the sea and produced a catastrophic tsunami, while at least 3.9×10^6 m^3 of the Assapaat frozen debris avalanche is assumed to have entered the sea, without causing a tsunami.

In and around the scarp area the two landslides are near-identical, but along their runout paths they differ. The difference in the two can be explained by the fact that part of the Niiortuut frozen debris avalanche was channelized, which we infer increased its mobility and tsunamigenic potential. This is a well-known phenomenon in the literature (Nicoletti and Sorriso-Valvo, 1991; Velardi et al., 2020).

A further aspect explaining why the Assapaat frozen debris avalanche did not produce a tsunami, is that it lost a lot of the initial kinetic energy, as it entrained a large dry volume of permafrozen material halfway down the slope, presumably because the permafrost here was at a critical temperature (see Svennevig et al., 2022). The energy of the initial frozen debris avalanche was not enough to accelerate the large, entrained volume sufficient for it to produce a tsunami. Furthermore, the slope gradient was low (15°) halfway down the slope where the entrainment occurred which also impaired the energy of the landslide. The Niiortuut frozen debris avalanche had no identifiable effect on its substrate along its runout path (no entrainment observed). We may speculate that this could be because the permafrozen lower slope was not susceptible to entrainment in 1952 as the permafrost here were not at a critical temperature at this point in time. When the Assapaat frozen debris avalanche occurred in 2021, the 69 years of continued warming of the permafrost may have caused the slope to be more susceptible to entrainment. Svennevig et al. (2022) suggested that as the slopes in the Arctic progressively warm and the permafrost degrades the dry entrainment observed in the Assapaat frozen debris avalanche may evolve into a wet entrainment that may increase the mobility, and thus the hazard, of future landslides.

The 2000 Paatuut rock avalanche, 17 km south-east of the Niiortuut frozen debris avalanche, was also channelized and produced a tsunami (Dahl-Jensen et al., 2004). Buchwal et al., 2015 specualted that this landslide was triggered by high seasonal rainfall. However, in the light of the findings presented here and the recent findings on the Assapaat frozen debris avalanche, a reassessment of the Paatuut rock avalanche is necessary to better understand the dynamics behind this, order of magnitude larger landslide.

4.4. Potential conditioning factors

It is difficult to Identify the preparing/dynamic conditioning (sensu Hermanns et al., 2006) and triggering factors for a landslide that has not been intensely monitored prior to failure and which occurred 70 years ago. The information available on the Niiortuut frozen debris avalanche in 1952 does not allow identification of what the dynamic conditioning factors for the landslide were with certainty. However, we can approach this from the available data which has been presented here. Field evidence such as the presence of hundreds of molards and thawing observed in the backscarp shows that the talus slope was permafrozen prior to failure. While the depth of the sliding surface was 80 m inside the talus slope (Fig. 6), it is commonly assumed that 10–15 m is the maximum depth where seasonal changes in temperature can affect permafrost (French,

2017). This points towards something with a longer amplitude than seasonality, such as permafrost degradation as a dynamic conditioning factor. As permafrost warmed to a critical temperature, the frictional shear stress of the interstitial ice drops and failure may occur. This has been shown to be the case in laboratory tests where the shear stress drops as temperature approaches the melting point (Davies et al., 2001; Krautblatter et al., 2013). In Arctic and subarctic environments, landslides mobilising loose material because of permafrost degradation, such as talus, rock glaciers or ice-cored moraines, are rarely reported in literature, but they all have analogue geomorphological features to the Niiortuut frozen debris avalanche, such as molards, lobate features, cracks opening in the source material showing signs of permafrost degradation (Brideau et al., 2010; Milana, 2016; Bodin et al., 2017; Morino et al., 2021; Sæmundsson et al., 2018). Permafrost degradation was also suggested as a conditioning factor for the 2021 Assapaat frozen debris avalanche (Svennevig et al., 2022).

Identifying triggering factors for the Niiortuut frozen debris avalanche is difficult. However, we can exclude seismicity, as there is no evidence that seismic events have triggered any of the other historic landslides in the area (Dahl-Jensen et al., 2004; Svennevig et al., 2020, 2022), which is known to be tectonically stable, with only few and minor earthquakes (Voss et al., 2007). As for weather conditions as a trigger, we know very little about the conditions when the landslide occurred. However, from the description in *Avangnâmiok* it is said that there was snow around the scarp area the day after the event, and that the temperature at sea level was freezing when the surviving fishermen walked to the hut after being hit by the waves. Thus, no clear weather dependant trigger, such as snowmelt or rain, can be identified from the limited sources. For the Assapaat frozen debris avalanche, water infiltration into the cracks produced by progressive creep caused by permafrost degradation was suggested as a trigger (Svennevig et al., 2022). However, no such supply of excess water was observed around the 1952 Niiortuut frozen debris avalanche and the timing of the triggering (15th December) is usually not a time of large snowmelt. Another possibility is that progressive permafrost degradation triggered the landslide, but the process behind these mechanisms is poorly understood and warrants more research.

4.5. Early onset of permafrost degradation

Given the general warming trend of the Arctic the past century (Overland et al., 2019), it is unsurprising that recent landslides in a region with continuous to discontinuous permafrost, such as the 2021 Assapaat frozen debris avalanche (Svennevig et al., 2022) and the 2009, 2016 and 2017 Karrat rock avalanches (Svennevig et al., 2020) may be attributed to permafrost degradation. We have shown that the Niiortuut frozen debris avalanche that occurred 69 years ago is pre-conditioned by the same processes as the recent Greenlandic landslides (warming of the slope). This may indicate that the slope reacted to the early twentieth century warming in the Arctic that initiated in the late 1910s. During this event, annual average Arctic temperatures peaked at a 1.7 °C anomaly in the period 1930–1940 with respect to previous decades (Bengtsson et al., 2004; Yamanouchi, 2011). This implies that these Arctic slopes might become prone to slope mass movements only after a couple of decades of warming. These speculations could be approached by applying permafrost models to the region to constrain the conditions in the slope prior to the failure of the Niiortuut frozen debris avalanche.

4.6. Hazard perspective in a warming climate

As mentioned above the Niiortuut and the Assapaat frozen debris avalanches are geomorphologically very similar. However, only one of them produced a deadly tsunami. From a hazard point of view, when analysing these phenomena, it is crucial to analyse the potential runout path. Is there potential for channelisation or entrainment? Is the potential entrainment wet or dry? Furthermore, if we accept that the difference in entrainment observed in the two landslides is a signal of the slopes warming during the 69 years between the two, then hazard assessment needs to change and adapt over time as conditions change. In this case the state of the permafrozen slope. This may be particularly important in areas with sporadic or continuous permafrost, where its state may cross a critical stability threshold as slopes continue to warm. Annual mean air temperature in the Arctic is projected (RCP 4.5) to increase by 7.5 °C by 2100 (IPCC, 2019) relative to the mean temperature from 1900 to 1950, and today the Arctic mean air temperature has increased by 2 °C since preindustrial time (Overland et al., 2019).

5. Conclusion

A 5.9×10^6 m^3 frozen debris avalanche occurred around 14:00 local West Greenland time on the 15th December 1952 near the Niiortuut mountain in Vaigat. Between 1.8×10^6 m^3 and 4.5×10^6 m^3 of material entered the Vaigat strait and generated a tsunami, with a recorded runup height of 2.2–2.7 m in the town of Qullissat, 30 km south-east of the landslide. The tsunami resulted in the death of a fisherman working approximately 10 km from the landslide and caused minor material damage in the Qullissat.

Our field based morphometric observations and interpretation of contemporaneous field and aerial photos show that the source area was in the talus slope and that the material involved was permafrost cemented talus. The frozen debris avalanche was conditioned by permafrost degradation in the talus slope similar to the recent 2021 Assapaat frozen debris avalanche 7 km to the south-east.

We infer that at the time of the failure permafrost in this region was already at a critical state after 3–4 decades of early twentieth century warming.

The Niiortuut frozen debris avalanche and other recent landslides in Greenland might be a sign that permafrost is increasingly degrading, and more landslides can be expected in the future as a result of continued warming.

CRediT authorship contribution statement

Kristian Svennevig: Conceptualization; Data curation; Formal analysis; Writing – original draft. **Marie Keiding:** Formal analysis, Writing - Review & Editing. **Niels Jákup Korsgaard:** Methodology: Historic DEMs, Writing - Review & Editing. **Antoine Lucas:** Methodology: recent DEM, Writing - Review & Editing. **Matthew Owen:** Methodology: Bathymetrical data, Writing - Review & Editing. **Majken Djurhuus Poulsen:** Methodology: Interviews, analysis and Greenlandic translation, Writing - Review & Editing. **Janina Priebe:** Investigation: historic/archival material, Writing - Review & Editing. **Erik Vest Sørensen:** Methodology: Historic and recent DEMs, Formal analysis: DEM of difference, Writing - Review & Editing. **Costanza Morino:** Morphological analysis of Molards, Writing - Review & Editing.

Data availability

Data will be made available on request.

Declaration of competing interest

The authors declare no competing interests.

Acknowledgements

A very special thanks are due to former residents of Qullissat and their descendants for providing valuable information on the landslide and tsunami. This paper is dedicated to them.

The governments of Denmark and Greenland funded the “Screening analysis of the risk for serious landslides in Greenland” in 2018, and the subsequent “Study of the risk for serious landslides in Greenland 2019-2022”, for which the original technical work was undertaken, including the marine investigation within Viagat strait. C. Morino and A. Lucas is funded by the Agence Nationale de la Recherche in the framework of the

project ANR-19-CE01-0010 PERMOLARDS. A. Lucas also acknowledges the support from the Programme National de Télédétection Spatiale (PNTS, grant N° PNTS-2022) and the LabEx UnivEarthS (ANR-10-LABX-0023 and ANR-18-IDEX-0001). The paper is published under permission of the Geological Survey of Denmark and Greenland (GEUS). Thanks are due to three anonymous reviewers for constructive comments.

References

Bengtsson, L., Semenov, V.A., Johannessen, O.M., 2004. The early twentieth-century warming in the arctic - a possible mechanism. J. Clim. 17, 4045–4057. https://doi.org/10.1175/1520-0442(2004)017<4045:TETWIT>2.0.CO;2.

Benjamin, J., Rosser, N.J., Dunning, S.A., Hardy, R.J., Kelfoun, K., Szczuciński, W., 2018. Transferability of a calibrated numerical model of rock avalanche run-out: application to 20 rock avalanches on the Nuussuaq Peninsula, West Greenland. Earth Surf. Process. Landforms https://doi.org/10.1002/esp.4469.

Bodin, X., Krysiecki, J., Schoeneich, P., Le Roux, O., Lorier, L., Echelard, T., Peyron, M., Walpersdorf, A., 2017. The 2006 collapse of the Bérard rock glacier (Southern french Alps). Permafr. Periglac. Process. 28, 209–223.

Brideau, M., Stead, D., Hopkinson, C., Demuth, M., Barlow, J., Evans, S., Delaney, K., 2010. Preliminary description and slope stability analyses of the 2008 little Salmon Lake and 2007 Mt.Steele landslides, Yukon. Yukon Explor. Geol. 119–134.

Buchwal, A., Szczuciński, W., Strzelecki, M.C., Long, A.J., 2015. New insights into the 21 November 2000 tsunami in West Greenland from analyses of the tree – ring structure of Salix glauca. Pol. Polar Res. 36, 51–65. https://doi.org/10.1515/popore.

Dahl-Jensen, T., Larsen, L.M., Pedersen, S.A.S., Pedersen, J., Jepsen, H.F., Pedersen, G.K., Nielsen, T., Pedersen, A.K., Von Platen-Hallermund, F., Weng, W.L., 2004. Landslide and tsunami 21 November 2000 in Paatuut,West Greenland. Nat. Hazards 31, 277–287. https://doi.org/10.1023/B:NHAZ.0000020264.70048.95.

Dam, G., Pedersen, G.K., Sønderholm, M., Midtgaard, H.H., Larsen, L.M., Nøhr-Hansen, H., Pedersen, A.K., 2009. Lithostratigraphy of the Cretaceous-Paleocene Nuussuaq Group, Nuussuaq Basin, West Greenland. Geol. Surv. Denmark Greenl. Bull. 19, 1–171. https://doi.org/10.34194/geusb.v19.4886.

Davies, M.C.R., Hamza, O., Harris, C., 2001. The effect of rise in mean annual temperature on the stability of rock slopes containing ice-filled discontinuities. Permafr. Periglac. Process. 12, 137–144. https://doi.org/10.1002/ppp 378.

French, H.M., 2017. The Periglacial Environment. 4th ed. Wiley, Blackwell, Hoboken, NJ.

Gariano, S.L., Guzzetti, F., 2016. Landslides in a changing climate. Earth-Sci.Rev. 162, 227–252. https://doi.org/10.1016/j.earscirev.2016.08.011.

Henriksen, N., Higgins, A.K., Kalsbeek, F., Pulvertaft, T.C.R., 2009. Greenland From Archaean to Quaternary Descriptive Text to the 1995 Geological Map of Greenland, 1:2 500 000, 2nd editionGeol. Surv. Denmark Greenl. Bull18, p. 126.

Hermanns, R.L., Niedermann, S., Villanueva Garcia, A., Schellenberger, A., 2006. Rock avalanching in the NW Argentine Andes as a result of complex interactions of lithologic, structural and topographic boundary conditions, climate change and active tectonics. In: Evans, S.G., Scarawcia Mugnozza, G., Strom, A.L., Hermanns, R.L. (Eds.), Landslides From Massive Rock Slope Failure. Springer, Netherlands, Celano, pp. 497–520.

Hermanns, R.L., Penna, I.M., Oppikofer, T., Noël, F., Velardi, G., 2021. Rock Avalanche. In: Shroder, J.F. (Ed.), Treatise on Geomorphology. Elsevier, p. 21 https://doi.org/10.1016/B978-0-12-818234-5.00183-8.

Higman, B., Shugar, D.H., Stark, C.P., Ekström, G., Koppes, M.N., Lynett, P., Dufresne, A., Haeussler, P.J., Geertsema, M., Gulick, S., Mattox, A., Venditti, J.G., Walton, M.A.L., McCall, N., Mckittrick, E., MacInnes, B., Bilderback, E.L., Tang, H., Willis, M.J., Richmond, B., Reece, R.S., Larsen, C., Olson, B., Capra, J., Ayca, A., Bloom, C., Williams, H., Bonno, D., Weiss, R., Keen, A., Skanavis, V., Loso, M., 2018. The 2015 landslide and tsunami in Taan Fiord,Alaska. Sci. Rep. 8, 1–13. https://doi.org/10.1038/s41598-018-30475-w.

Hungr, O., Evans, S.G., 2004. Entrainment of debris in rock avalanches: an analysis of a long run-out mechanism. GSA Bull. 116, 1240–1252. https://doi.org/10.1130/B25362.1.

Hungr, O., Leroueil, S., Picarelli, L., 2014. The varnes classification of landslide types, an update. Landslides 11, 167–194. https://doi.org/10.1007/s10346-013-0436-y.

IPCC, 2019. In: Pörtner, H.-O., Roberts, D.C., Masson-Delmotte, V., Zhai, P., Tignor, M., Poloczanska, E., Mintenbeck, K., Alegría, A., Nicolai, M., Okem, A., Petzold, J., Rama, B., Weyer, N.M. (Eds.), Special report on the ocean and cryosphere in a changing climate.

Krautblatter, M., Funk, D., Günzel, F.K., 2013. Why permafrost rocks become unstable: a rock–ice-mechanical model in time and space. Earth Surf. Process. Landforms 38, 876–887. https://doi.org/10.1002/esp.3374.

Milana, J.P., 2016. Molards and their relation to landslides involving permafrost failure. Permafr. Periglac. Process. 27, 271–284. https://doi.org/10.1002/ppp.1878.

Morino, C., Conway, S.J., Balme, M.R., Helgason, J.K., Sæmundsson, Þ., Jordan, C., Hillier, J., Argles, T., 2021. The impact of ground-ice thaw on landslide geomorphology and dynamics: two case studies in northern Iceland. Landslides 1–28.

Morino, C., Conway, S.J., Sæmundsson, Þ., Kristinn, J., Hillier, J., Butcher, F.E.G., Balme, M.R., Jordan, C., Argles, T., Kristinn Helgason, J., Hillier, J., Butcher, F.E.G., Balme, M.R., Jordan, C., Argles, T., 2019. Molards as an indicator of permafrost degradation and landslide processes. Earth Planet. Sci. Lett. 516, 136–147. https://doi.org/10.1016/j.epsl.2019.03.040.

Nicoletti, P.G., Sorriso-Valvo, M., 1991. Geomorphic controls of the shape and mobility of rock avalanches. Geol. Soc. Am. Bull. 103, 1365–1373. https://doi.org/10.1130/0016-7606(1991)103<1365:GCOTSA>2.3.CO;2.

Oppikofer, T., Hermanns, R.L., Roberts, J., Böhme, M., 2018. SPLASH: semi-empirical prediction of landslide-generated displacement wave run-up heights. Geol. Soc. Spec. Publ. 477, 14. https://doi.org/10.1144/SP477.1.

Oppikofer, T., Saintot, A., Hermanns, R.L., Böhme, M., Scheiber, T., Gosse, J., Dreiås, G.M., 2017. From incipient slope instability through slope deformation to catastrophic failure — different stages of failure development on the ivasnasen and vollan rock slopes (western Norway). Geomorphology 289, 96–116. https://doi.org/10.1016/j.geomorph.2017.03.015.

Overland, J., Dunlea, E., Box, J.E., Corell, R., Forsius, M., Kattsov, V., Skovgård, M., Pawlak, J., Reiersen, L., Wang, M., Pacific, N., Environmental, M., States, U., 2019. The urgency of Arctic change. Polar Sci. 21, 6–13. https://doi.org/10.1016/j.polar.2018.11.008.

Paris, A., Okal, E.A., Guérin, C., Heinrich, P., Schindelé, F., Hébert, H., 2019. Numerical modeling of the june 17, 2017 landslide and tsunami events in Karrat Fjord,West Greenland. Pure Appl. Geophys. 176, 3035–3057. https://doi.org/10.1007/s00024-019-02123-5.

Patton, A.I., Rathburn, S.L., Capps, D.M., 2019. Landslide response to climate change in permafrost regions. Geomorphology 340, 116–128. https://doi.org/10.1016/j.geomorph.2019.04.029.

Pedersen, A.K., Larsen, L.M., Pedersen, G.K., 2018. Lithostratigraphy, geology and geochemistry of the volcanic rocks of the Maligât Formation and associated intrusions on Disko and Nuussuaq, Paleocene of West Greenland. Geol. Surv. Denmark Greenl. Bull. 40, 1–239. https://doi.org/10.34194/geusb.v40.4326.

Pedersen, A.K., Larsen, L.M., Pedersen, G.K., 2017. Lithostratigraphy, geology and geochemistry of the volcanic rocks of the Vaigat Formation on Disko and Nuussuaq, Paleocene of West Greenland. Geol. Surv. Denmark Greenl. Bull. 39, 1–244. https://doi.org/10.34194/geusb.v39.4354.

Pedersen, A.K., Larsen, L.M., Ulff-Møller, F., Pedersen, G.K., Dueholm, K.S., 2001. Geolgical Map of Greenland, 1:100 000, Pingu 69 V.2 Nord.

Pedersen, A.K., Pedersen, G.K., Larsen, L.M., Pulvertaft, T.C.R., Sønderholm, M., Dueholm, K.S., 2007. Geological Map of the Nuussuaq Basin in Southern Nuussuaq, 1:100 000, Special Map Paatuut, With Detailed Sections. Geological Survey of Denmark and Greenland, Copenhagen.

Pedersen, S.A.S., Larsen, L.M., Dahl-jensen, T., Jepsen, H.F., Krarup, G., Nielsen, T., Pedersen, A.K., Von Platen-Hallermund, F., Weng, W.L., 2002. Tsunami-generating rock fall and landslide on the south coast of Nuussuaq, central West Greenland. Geol. Greenl. Surv. Bull. 191, 73–83.

Ribergaard, M.H., 2022. Tide Tables for Greenlandic Waters 2023, DMI Report. Copenhagen 2022. https://doi.org/10.1093/nq/s1-VII.172.156-a.

Rosenkrantz, A., Münther, V., Henderson, G., Pedersen, A.K., Hald, N., 1976. Geological Map of Greenland, 1:100 000, Qutdligssat 70 V.1 Syd. Grønlands Geologiske Undersøgelse, København.

Sæmundsson, Þ., Morino, C., Conway, S.J., 2021. Mass-movements in cold and polar climates. In: Shroder, J.F. (Ed.), Treatise on Geomorphology. Elsevier, p. 21 https://doi.org/10.1016/B978-0-12-818234-5.00117-6.

Sæmundsson, Þ., Morino, C., Helgason, J.K., Conway, S.J., Pétursson, H.G., 2018. The triggering factors of the Móafellshyrna debris slide in northern Iceland: intense precipitation, earthquake activity and thawing of mountain permafrost. Sci. Total Environ. 621, 1163–1175. https://doi.org/10.1016/j.scitotenv.2017.10.111.

Schleier, M., Hermanns, R.L., Rohn, J., Gosse, J.C., 2015. Diagnostic characteristics and paleodynamics of supraglacial rock avalanches, Innerdalen, Western Norway. Geomorphology 245, 23–39. https://doi.org/10.1016/j.geomorph.2015.04.033.

Sepulveda, S.A., Serey, A., Lara, M., Pavez, A., Rebolledo, S., 2010. Landslides induced by the April 2007 Aysén Fjord earthquake, Chilean Patagonia. Landslides 7, 483–492. https://doi.org/10.1007/s10346-010-0203-2.

Strzelecki, M.C., Jaskólski, M.W., 2020. Arctic tsunamis threaten coastal landscapes and communities -Survey of Karrat Isfjord 2017 tsunami effects in Nuugaatsiaq, western Greenland. Nat. Hazards Earth Syst. Sci. 20, 2521–2534. https://doi.org/10.5194/nhess-20-2521-2020.

Svennevig, K., 2019. Preliminary landslide mapping in Greenland. Geol. Surv. Denmark Greenl. Bull. 43, e2019430207. https://doi.org/10.34194/geusb-201943-02-07.

Svennevig, K., Dahl-Jensen, T., Keiding, M., Boncori, J.P.M., Larsen, T., Salehi, S., Solgaard, A.M., Voss, P.H., 2020. Evolution of events before and after the 17 June 2017 rock avalanche at Karrat Fjord, West Greenland – a multidisciplinary approach to detecting and locating unstable rock slopes in a remote Arctic area. Earth Surf. Dyn. 8, 1021–1038. https://doi.org/10.5194/esurf-8-1021-2020.

Svennevig, K., Hermanns, R.L., Keiding, M., Binder, D., Citterio, M., Dahl-Jensen, T., Mertl, S., Sørensen, E.V., Voss, P.H., 2022. A large frozen debris avalanche entraining warming permafrost ground—the June 2021 Assapaat landslide, West Greenland. Landslides https://doi.org/10.1007/s10346-022-01922-7.

Velardi, G., Hermanns, R.L., Penna, I., Böhme, M., 2020. Prediction of the reach of rock slope failures based on empirical data from Norway. ISRM Int. Symp. - EUROCK 2020.

Voss, P.H., Poulsen, K., Simonsen, S.B., Gregersen, S., 2007. Seismic hazard assessment of Greenland. Geol. Surv. Denmark Greenl. Bull. 13, 57–60. https://doi.org/10.34194/geusb.v13.4976.

Weidick, A., 1992. Landhævning og landsænkning i Grønland siden sidste istid. Naturens Verden 3, 81–96.

Weidick, A., Bennike, O., 2007. Quaternary glaciation history and glaciology of Jakobshavn Isbræ and the Disko Bugt region, West Greenland: a review. Geol. Surv. Denmark Greenl. Bull. 14, 80.

Westergaard-Nielsen, A., Karami, M., Hansen, B.U., Westermann, S., Elberling, B., 2018. Contrasting temperature trends across the ice-free part of Greenland. Sci. Rep. 8, 1–6. https://doi.org/10.1038/s41598-018-19992-w.

Yamanouchi, T., 2011. Early 20th century warming in the Arctic: a review. Polar Sci. 5, 53–71. https://doi.org/10.1016/j.polar.2010.10.002.